

From structure mining to unsupervised exploration of atomic octahedral networks

R. Patrick Xian,^{*,†,‡} Ryan J. Morelock,^{¶,⊥} Ido Hadar,[§]
Charles B. Musgrave,^{¶,#} and Christopher Sutton^{*,†,||}

[†]*Department of Engineering, University of Cambridge, Trumpington Street,
Cambridge CB2 1PZ, United Kingdom.*

[‡]*Department of Chemistry and Biochemistry, University of South Carolina, 631 Sumter Street,
Columbia, SC 29208, USA.*

[¶]*Department of Chemical and Biological Engineering, University of Colorado Boulder,
3415 Colorado Avenue, Boulder, CO 80303, USA.*

[§]*The Institute of Chemistry, Casali Center for Applied Chemistry, and the Center for Nanoscience
and Nanotechnology, The Hebrew University of Jerusalem, Edmond J. Safra Campus, Givat-Ram,
9190401 Jerusalem, Israel.*

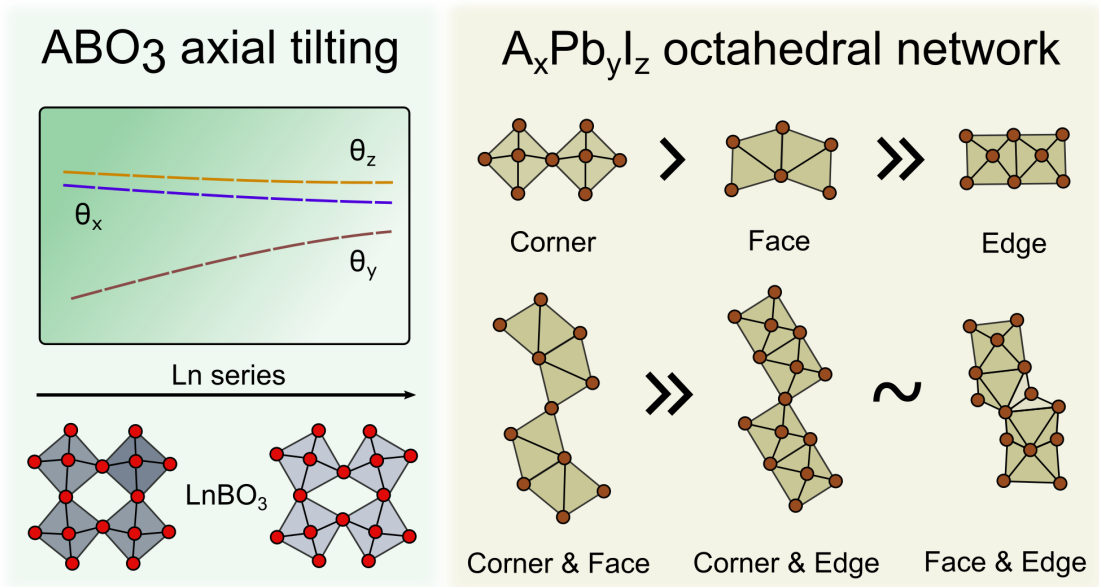
^{||}*Department of Materials Science and Engineering, University of Toronto, 184 College Street,
Toronto, ON M5S 3E4, Canada.*

[⊥]*Current address: Center for Nanophase Materials Science, Oak Ridge National Laboratory,
1 Bethel Valley Road, Oak Ridge, TN 37831, USA.*

[#]*Current address: John and Marcia Price College of Engineering, University of Utah,
72 S. Central Campus Drive, Salt Lake City, UT 84112, USA.*

E-mail: xpatrick@gmail.com; ca.sutton@utoronto.ca

Understanding the spatial arrangements of atom-centered coordination octahedra is crucial for relating structures to properties for many materials families. Traditional case-by-case inspection becomes a prohibitive task for discovering trends and similarities in large datasets. Here, we operationalize chemical intuition to automate the geometric parsing, quantification, and classification of coordination octahedral networks using unsupervised machine learning. We apply the workflow to analyze two datasets to demonstrate its effectiveness. For computationally generated single oxide perovskite (ABO_3) polymorphs, we uncover axis-dependent tilting trends which assist in detecting oxidation state changes. For hybrid iodoplumbates ($A_xPb_yI_z$) from measured structures, we taxonomize their octahedral networks, revealing a Pauling-like connectivity rule for the coordination environment and the design principles underpinning their structural diversity. Our results offer a glimpse into the vast design space of atomic octahedral networks in materials chemistry and inform high-throughput, targeted screening of specific structure types.



Highlights of the two case studies in this work on the computational analysis of materials distinguished by their octahedral networks. Left: Axis-resolved tilting trends from A-site substitution in lanthanide oxide perovskite series ($LnBO_3$). Right: Pauling-like rules for the prevalence of connectivity patterns among the inorganic polytypes of hybrid iodoplumbates ($A_xPb_yI_z$).

Introduction

The coordination polyhedron is a recurring theme in chemistry from molecules to solids.¹⁻⁶ Among inorganic compounds, coordination octahedra (COs) are one of the most common local atomic environments of metal-centered ions.⁷ Octahedral networks (ONs, i.e., networks of COs) display elaborate spatial patterns based on orientation (i.e., tilting), distortion, and connectivity, which underlie the stability and functionalities of materials. The most prominent representatives of materials containing ONs belong to the perovskite structure family.⁸

Besides the corner-sharing ONs in classic perovskites, their variants are prevalent in binary and multinary compounds,^{1,2,9,10} metal-rich clusters¹¹ (with anion-centered COs), numerous hydroxide-based crystalline minerals,^{5,6} and functional materials,¹²⁻¹⁵ etc. Incidentally, ONs are also a convenient abstraction of the underlying atomistic identity and are enumerable algorithmically,⁵ providing an intuitive surrogate to first-principles approaches for explaining the mechanisms leading to outstanding material properties.^{16,17} Therefore, it is not an understatement that cataloging and documenting the architecture and distribution of ONs greatly facilitates our understanding of matter.^{3,18}

Designing materials that contain ONs may be viewed through the lens of spatial patterning or tiling. Although the ON design space extends in multiple directions,¹⁹ in this work, we computationally examined two dimensions: chemical diversity and network connectivity, as illustrated in Fig. 1a, taking the perovskite family of materials as examples. Along the chemical diversity axis, alloying multiple ions can create new properties. Single perovskites have the formula unit ABX_3 , where A and B are cations, and X is an anion. The oxide single perovskites (ABO_3), which are well-studied, has a total member count approaching 5×10^3 . This number quickly explodes to 10^7 for double oxide perovskites ($AA'BB'O_6$)²⁰⁻²² and much more for higher-order multinary perovskites. The connectivity within the ONs may be modified by pairing with selected organic cations in these structures, which in turn alter the structural stability and electronic properties without tuning the chemical diversity of the ON. This results in the distinctive connectivity patterns that characterize the hybrid (i.e., containing both organic and inorganic parts) perovskites and their extended families of materials, called perovskitoid or hybrid metalates.^{13,23-26}

Existing methods for quantifying ONs in chemical structures date back at least half a century: The Glazer tilt system proposed in the 1970s²⁹ classifies the spatial orientation of corner-sharing COs in perovskites and is widely adopted by the community. The periodic nets introduced by Wells from the 1950s to the 1970s^{2,18} and the structural hierarchy hypothesis introduced by Hawthorne shortly afterwards⁵ provide an intuitive simplification of the ONs for understanding their similarity and complexity. In recent decades, advances in chemical synthesis have greatly expanded the diversity of compounds containing ONs (see Fig. 1b), which exhibit seemingly unlimited possible arrangements. Although the classification nomenclature for these modular structures is still under

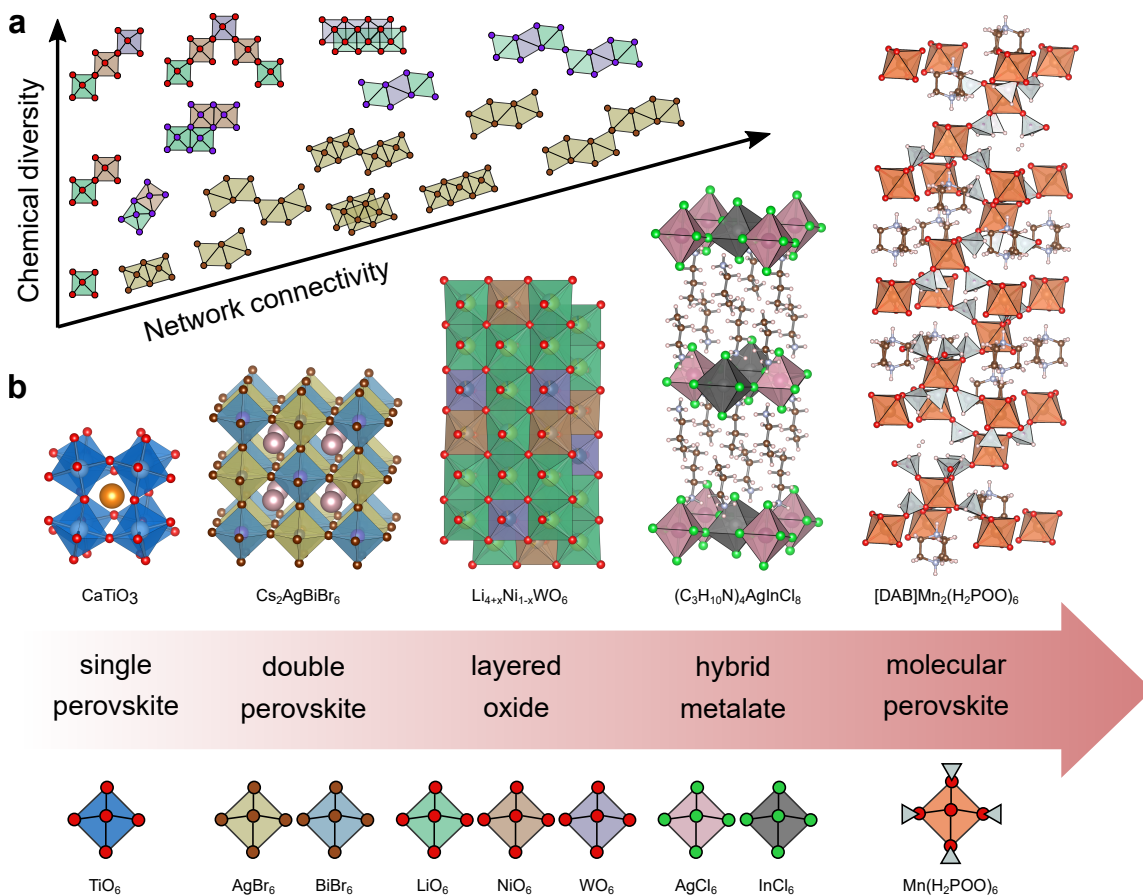


Figure 1: Spatial complexity of octahedral networks. **a**, Illustration of the spatial complexity of octahedral networks (ONs) along two directions: chemical diversity and network connectivity. The difference in chemical composition is represented by color. The types of connectivity between octahedra are categorized as corner-, edge-, and face-sharing. **b**, A progression of exemplary materials containing ONs is shown from left to right. The structures are taken from materials databases (single perovskite CaTiO₃) and publications (double perovskite Cs₂AgBiBr₆, layered nonstoichiometric oxide Li_{4+x}Ni_{1-x}WO₆,²⁷ hybrid multinary perovskite (C₃H₁₀N)₄AgInCl₈,¹⁴ and molecular perovskite [DAB]Mn₂(H₂POO)₆²⁸). The legend at the bottom indicates the types of coordination octahedra present in the corresponding crystal structures directly above each octahedron.

active debate, the materials families containing ONs are increasingly viewed as a continuum with shared chemical provenance and connectivity patterns.^{30,31} Moreover, modern atomic-resolution electron microscopy is capable of characterizing local disordering at heterogeneous interfaces,³² creating opportunities to broadly sample the configurational space and cross-examine experimental results with theoretical predictions. Driven by the growing quantity of structural data and the community efforts towards developing compact and efficient representations of molecular and materials systems,^{33,34} we present here a computational workflow for the structural analysis and discovery of atomic ONs to obtain summary statistics and occurrence ranking. These are enabled by geometry processing,³⁵ unsupervised machine learning (manifold learning and clustering), and

human label refinement with the use of a coordination network encoding (CNE) scheme with scale invariance. The collection of these methods reveals the octahedral tilting trends in oxide perovskite polymorphs and guides the identification of inorganic polytypes in hybrid iodoplumbates (i.e., lead iodide salts), which led us to discover the preference of connectivity in contrast with Pauling’s third rule^{1,36} in these materials and the power-law distribution of polytypes.

Results

We developed an atomic structure parsing workflow (see SI section 1) to analyze ONs using two graphs: (i) the mesh graph which uses atoms as nodes and involves the outer surface of the coordination polyhedra; (ii) the inter-unit graph which uses the COs as the nodes. The mesh graph provides connectivity information at the atomic level, while the inter-unit graph includes the connectivity information for the COs. They capture the hierarchical information in the ONs and provide the basis for analyzing large materials structure datasets involving ONs to gain insights into the design principles of complex (e.g., multivalent) perovskites and hybrid perovskite-derived materials. In the following, we present the results on oxide perovskite and hybrid iodoplumbate datasets.

Octahedral tilting in oxide perovskite (ABO_3) polymorphs

The discussions on octahedral tilting trends are normally based on the examination of specific subclasses of single perovskite structures that have been synthesized.^{16,37} Proxies for the tilting angle,^{38–40} such as the B-O-B angle, have often been used to estimate the octahedra orientation, and typically only small datasets of experimental data⁴¹ have been examined in attempts to uncover trends between these proxies and materials properties. However, a large proportion of the abundant oxide perovskites found on earth persist in kinetically trapped metastable states, either as polymorphs with free energies above the convex hull vs. composition phase diagram or as precursors or intermediates that form during chemical synthesis.⁴² Consequently, understanding the large design space of oxide perovskites requires evaluating many configurations, including those of metastable polymorphs.

The structure mining workflow we constructed leads to a more complete picture, along with the availability of a large dataset of oxide perovskite polymorphs from high-throughput computation⁴⁴ (see SI section 2). The dataset includes a total of over 2000 structures (see Methods) divided into ten different Glazer tilt classes.²⁹ We illustrate our results in Fig. 2 using orthorhombic polymorphs in the $a^+b^-b^-$ (#10) tilt class, while additional information is provided in SI section 2. Two distinctive trends stand out in Fig. 2: (1) There exists a clear dependence (the global trends) of tilt-

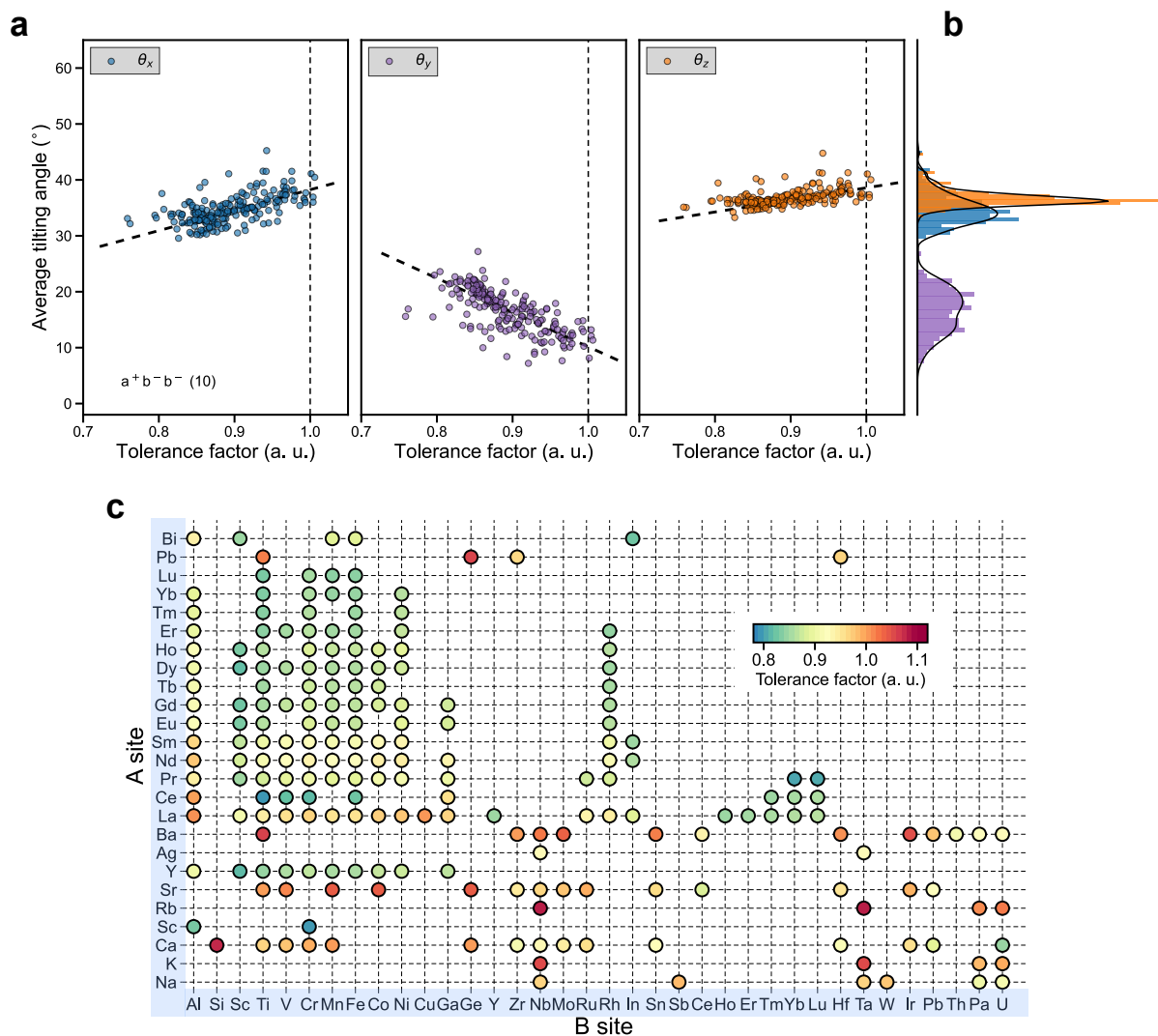


Figure 2: **Octahedral tilting trends in orthorhombic ABO_3 polymorphs.** **a**, Dependence on the Goldschmidt tolerance factor⁴³ for the axis-dependent tilting angles of single oxide perovskite polymorphs within the tilt class $a^+b^-b^-$ (#10). The dashed lines highlight the linear trend. The density estimation is shown in **b** with corresponding colors. **c**, Map of the Goldschmidt tolerance factor through the computationally accessed chemical space.

ing angles on the Goldschmidt tolerance factor⁴³ for almost all non-cubic polymorphs; (2) When ranked by the periodicity of the elements, we observe repeating patterns (the microtrends) of the tilting angles. The observation indicates that, in certain classes of polymorphs, the atomic structures obtained through isovalent substitution of *A*-site (or *B*-site) cations are highly predictable, which gives rise to a periodic table of oxide perovskite polymorphs. These microtrends reflect the dependence of chemical substitution on the structure (or property) in a substitution series.

A closer look at the *A*-site substitution series (Fig. 3a), such as lanthanide metalates (LnBO_3), reveals a monotonic change in all tilting angles as the ionic radius decreases (the lanthanide con-

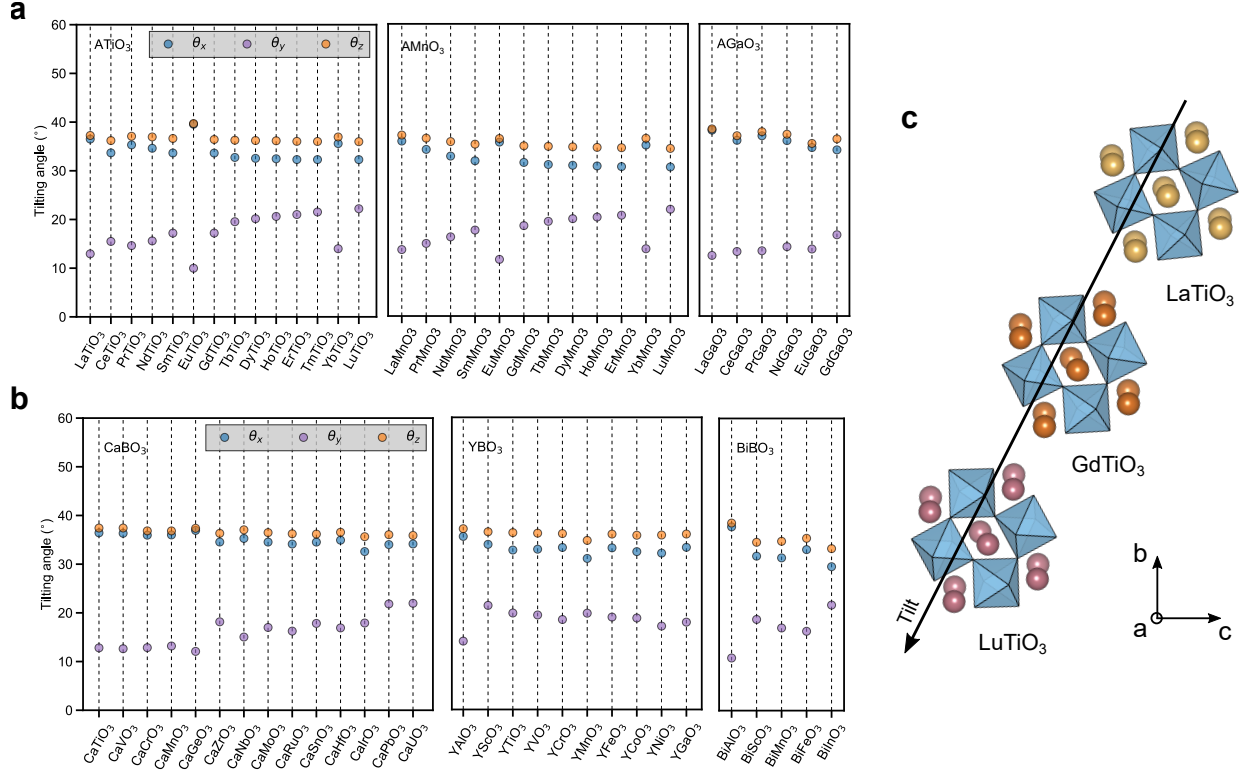


Figure 3: **Axis-dependent tilting in ABO₃ substitution series.** Microtrends of axis-dependent octahedral tilting found for representative *A*-site (a) and *B*-site (b) cation substitution series. c, An example series of lanthanide oxide perovskite structures exhibiting tilting microtrends. The three structures shown here are orthorhombic LaTiO₃, GdTiO₃, and LuTiO₃ with the TiO₆ coordination octahedra colored in light blue. The structures are displayed along the crystallographic *a* axis as indicated in the compass.

traction). These microtrends are similar in orthorhombic lanthanide titanates (LnTiO₃), manganites (LnMnO₃), and gallates (LnGaO₃). The structural changes also correlate with the changes in their experimental properties as previously reported.^{45,46} In *B*-site substitution series (see Fig. 3b), a similar pattern emerges, albeit across a broader range of substituted cations. These tilting microtrends within a large dataset can identify outlier materials directly based on their structural deviations. In the case of oxide perovskites, we find that the europium and ytterbium perovskites break the tilting trends (see Fig. 3a). Subsequent charge analysis of all cations (see SI section 2) in the orthorhombic LnTiO₃ and LnMnO₃ series using DFT+U onsite magnetic moments show that europium and ytterbium ions are in the +2 oxidation state, forming divalent-tetravalent perovskites (A²⁺B⁴⁺O₃), whereas the remaining compounds in the series are trivalent perovskites (A³⁺B³⁺O₃). Typically, assigning oxidation states in large computational screening datasets is a complicated task, but our analysis shows that the structural trend obtained from COs is a convenient indicator for changes in the oxidation state of cations.

Octahedral network motifs in hybrid iodoplumbates ($A_xPb_yI_z$)

Small organic molecules have been traditionally used to template the ON,⁴⁷ resulting in a wide range of modular (or recombination) structures^{4,48} with a multimeric ON as the inorganic framework. A multimeric ON contains more than a single CO in its motif. Besides complex oxides,⁴⁹ hybrid metalates²⁵ such as iodoplumbates are prominent examples. Existing terminologies used to describe the ON connectivity pattern are unstructured. For example, purely corner-sharing network motifs are classified by (i) the cleaving plane index,^{13,47} (ii) homologous series,^{50,51} which contain stacked octahedral layers of varying thickness, and (iii) corrugated network,⁵² which contains W-shaped octahedral sequences with mixed *cis* and *trans* neighbor configurations. These classification conventions are mostly derived from the crystallographic shear structures.¹⁷ Moreover, the umbrella term *perovskitoid* from the halide perovskite community^{23,26} was originally used to denote 1D structures with face-sharing octahedra, but now generally refers to the extended family of hybrid metalates without purely corner-sharing ONs. In general, these attempts lack specificity in capturing the variety of low-dimensional structures and are incompatible with high-throughput computational screening.

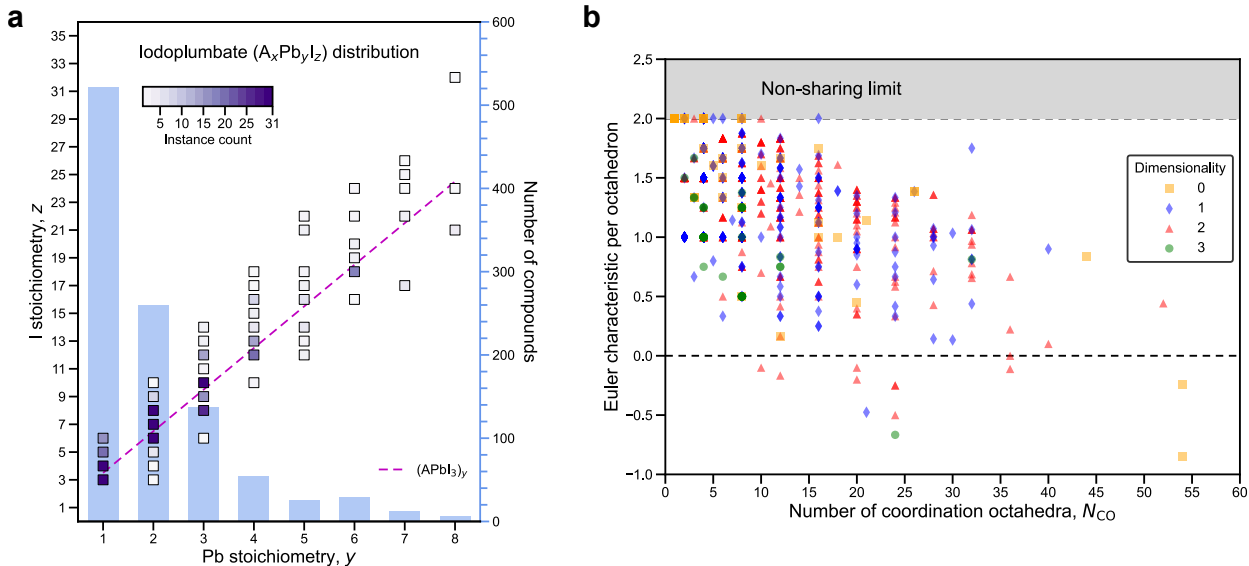


Figure 4: **Landscape of iodoplumbate octahedral networks.** **a**, Existing stoichiometries of hybrid iodoplumbates ($A_xPb_yI_z$) mined from the Cambridge Structural Database. **b**, Relationship between the number of coordination octahedra (N_{CO}) and the Euler characteristic per octahedron (χ^{ON}/N_{CO}). Each point represents an example of hybrid iodoplumbates, colored according to the framework dimensionality⁵³ of the material.

Previous attempts at linking stoichiometry to dimensionality^{54,55} showed limited success in small case studies^{56,57} and became less effective with the increasing complexity of the materials design space. In our view, the limitation is due to the restricted feature space and problem formula-

tion (i.e., predicting dimensionality using stoichiometry). A taxonomy should also distinguish the topological aspect of the structural components,⁵⁸ which is equivalent to polymorph (or polytype) identification. Our procedure builds on these requirements for motif assignment in hybrid metalates, which aims to distinguish the inorganic polytypes, regardless of the organic constituent. To this end, we analyzed ~ 970 compounds from the Cambridge Structural Database that are hybrid iodoplumbates (see Methods), $A_xPb_yI_z$, where A is an organic cation, and the $[Pb_yI_z]^{n-}$ polynuclear anion induces polytypism. The hybrid iodoplumbates are the most studied members of the hybrid metalate materials family that also includes hybrid perovskites.^{25,54,55}

Structure mining of $A_xPb_yI_z$. We first explored the stoichiometric and topological diversity of $A_xPb_yI_z$ compounds using our computational workflow. In Fig. 4a, the stoichiometric ratio between lead (Pb) and iodine (I) in the empirical formula is on the order of 3:1, yielding an average formula of $(APbI_3)_y$. As the number of Pb atoms in the formula unit increases, so does the scatter along the magenta dashed line representing $z \sim 3y$, indicating stoichiometries that more frequently deviate from this 3:1 ratio due to the growing complexity of network connectivity. When representing the polynuclear anions ($[Pb_yI_z]^{n-}$, with n being the charge it bears) by 3D meshes, we can calculate the relationship between the number of COs and the Euler characteristic^{59,60} of the mesh graph representing the ONs (see SI section 1). The results in Fig. 4b lie within a region bounded by the non-sharing limit, where isolated octahedra (i.e., 0D hybrid perovskites⁶¹) exist. The Euler characteristic is an invariant metric for topological objects. For convex shapes such as single convex octahedra, it attains a value of 2, while it becomes less than 2 for nonconvex shapes.^{59,60} Fig. 4b shows that as the number of COs increases, the Euler characteristic generally decreases in value, indicating a departure from convex shapes, as a result of atom-sharing between neighboring COs. This observation supports the use of topological features to distinguish between inorganic polytypes.

Clustering with CNE representation. The CNE is a vector representation of the ON constructed with the stoichiometric and topological information of the Pb_yI_z motif (see SI section 3). We perform dimensionality reduction and clustering interactively to identify the distribution of polytypes, as shown in Fig. 5a. Manifold learning is used here for dimensionality reduction because it provides an interpretable (due to well-separated clusters) visualization⁶² of underlying structures of the dataset to facilitate subsequent clustering. We validate the clusters derived from the algorithms using both external and internal metrics, along with polytype labels generated by visualization and human refinement (see Tables S3-S6). The clusters within the $A_xPb_yI_z$ dataset⁶³ uncovered here correspond to structures with a shared ON motif. Details of the procedure are provided in SI section 3. We rank the inorganic polytypes according to their occurrence in the dataset, revealing a double Pareto behavior (i.e., power-law relation involving two regimes)⁶⁴, as in Fig. 6a, and the top-twenty entries (out of ~ 70) are listed in Fig. 5b. The existence of two power-law

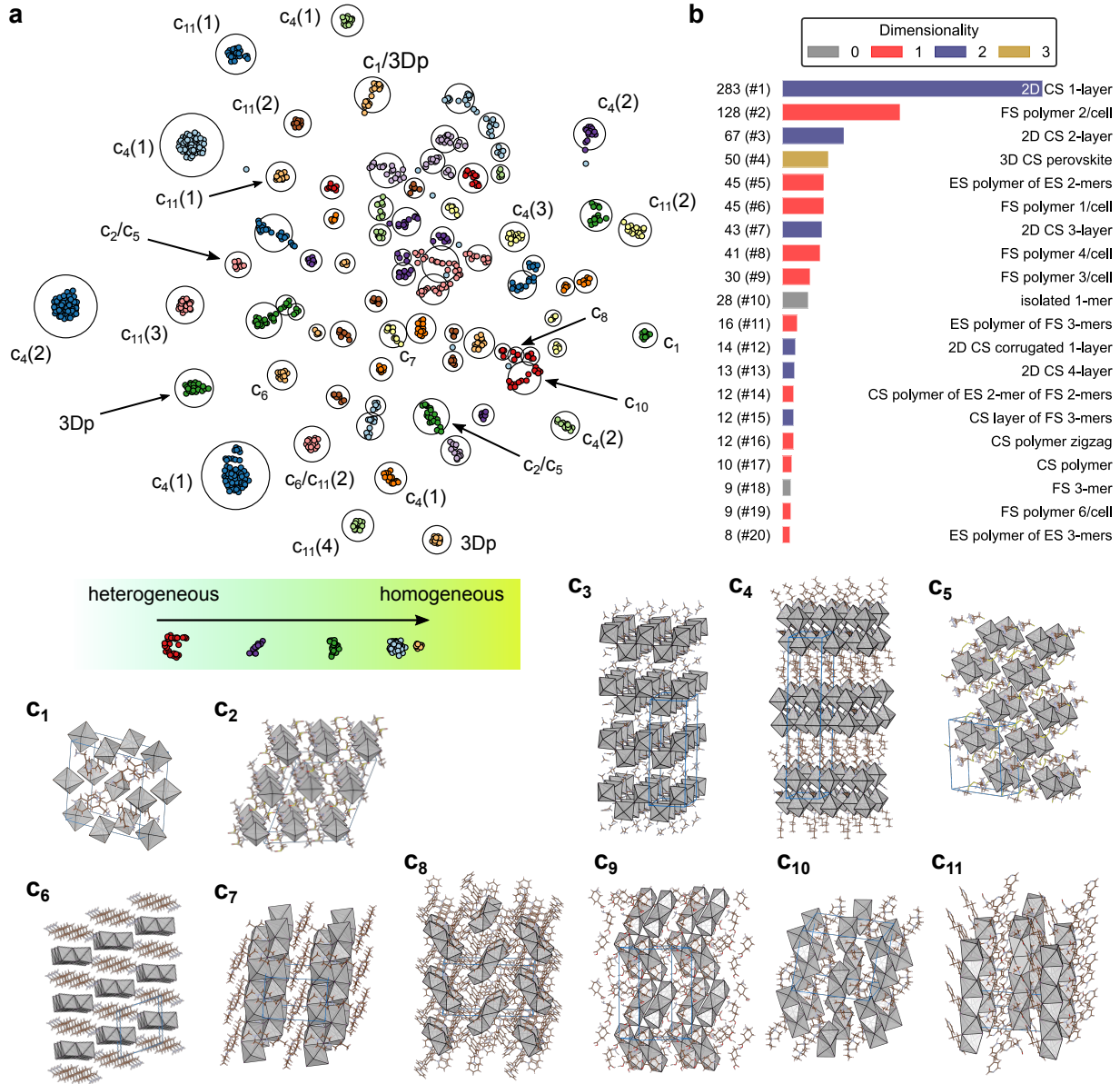


Figure 5: **Computational taxonomy of octahedral networks in $A_xPb_yI_z$.** **a**, Embedding space visualization of Pb_yI_z octahedral networks. Some of the major clusters are labeled with shorthand notations in connection to **c**. The number in parentheses indicates the number of building units per unit cell. The black circles and the colors distinguish the identified clusters from unsupervised machine learning. **b**, The top twenty polytypes in the occurrence ranking derived from the clustering in **a** and human label refinement. The colors in the bar chart represent the grouping by dimensionality. The representative structures are shown in **c₁**-**c₁₁**, from monomeric to polymeric octahedral networks with diverse motifs. The names of the motifs are **c₁**, non-sharing 1-mer (0D perovskite), **c₂**, straight CS 2-layer; **c₃**, corrugated CS 1-layer; **c₄**, straight CS chain; **c₅**, corrugated CS chain; **c₆**, ES chain of ES 2-mers; **c₇**, CS chain of ES 2-mer of FS 2-mers; **c₈**, isolated FS 3-mers; **c₉**, CS layer of FS 3-mers; **c₁₀**, ES chain of FS 3-mers; **c₁₁**, FS chain. In terms of framework dimensionality, polytype **c₁** and **c₈** are 0D, polytype **c₂**, **c₅**, **c₆**, **c₇**, **c₁₀**, **c₁₁** are 1D, polytype **c₃**, **c₄**, **c₉** are 2D. The solid blue box outlines the unit cell of the respective structure.

coefficients indicates distinct regimes. Here, they are most likely a result of the selective research activities associated with these materials that distinguish the common from the rare polytypes. The common polytypes are chemically fine-tuned to improve their key properties. Whereas the rare polytypes appear in unique studies or are characterized as intermediate products in chemical fine-tuning.^{26,65,66} Some of the prominent polytypes are visualized by their examples in Fig. 5c.

We find that a number of clusters already show high purity in Fig. 5a, where homogeneous clusters tend to have a more globular shape than heterogeneous ones. The shorthand notations in 5a correspond to the indices in Fig. 5c and its potential variants. For example, $c_4(1)$ indicates CS 1-layer polytype, or single-layer 2D hybrid perovskite, $c_{11}(2)$ indicates having the FS chain polytype with two independent chains per unit cell, 3Dp represents 3D CS hybrid perovskites. Clusters with two major polytypes are indicated with a slash, such as c_2/c_5 . A complete description of the naming rules for the polytypes is provided in Methods. More examples for the identified inorganic polytypes are provided in Table S5.

The major clusters in Fig. 5a represent common network motifs: CS k -layers (of different layer thickness k), FS chains (with different numbers of polymeric chains per unit cell), 0D and 3D hybrid perovskite structures. Some of the lesser-known polytypes are also aggregated into high-purity clusters, including those with mixed connectivity such as ES chain of FS 3-mers (Fig. 5c₁₀), CS layer of FS 3-mers (Fig. 5c₉), and CS chain of ES 2-mer of FS 2-mers (Fig. 5c₇), which has a 1D arrangement of COs similar to the columnar substructure of the V_2O_3 corundum (see Fig. 7).^{67,68} Although the mixed connectivity in this polytype due to the $[Pb_2I_6]^{2-}$ anion is in seeming violation of Pauling’s third rule, it’s surprisingly more common than many other inorganic polytypes found in the $A_xPb_yI_z$ dataset. A caveat to mention is that the clusters in Fig. 5c with the same label generally differ in the packing of the organic cation and its charge (n/x for $[A_x]^{n+}$), which is not considered explicitly in polytype identification but emerges due to the correlation between the characteristics of the organic cation and the inorganic framework it supports. Chemically speaking, the organic packing is a part of the structural motifs of these materials, but is not the network motif of the PbI_6 COs.

Moreover, we compare the effectiveness of the CNE with an established atom-centered representation, the smooth overlap of atomic positions (SOAP),⁶⁹ a kernel-based symmetry-invariant representation that prioritizes distance information, which has been used to visualize materials design spaces.⁷⁰ The results from our controlled numerical experiments (see Fig. S6 and Table S4) show that, because of the scale dependence of the kernel, clusters from the SOAP representation⁶⁹ are generally less pure than those obtained from the CNE scheme, and exhibit more elongated shapes, which are less beneficial for the subsequent polytype identification.

Pauling-like rules for iodoplumbates. The statistical summary of identified polytypes shows that in hybrid iodoplumbates, a significant proportion of existing materials contain only CS or FS

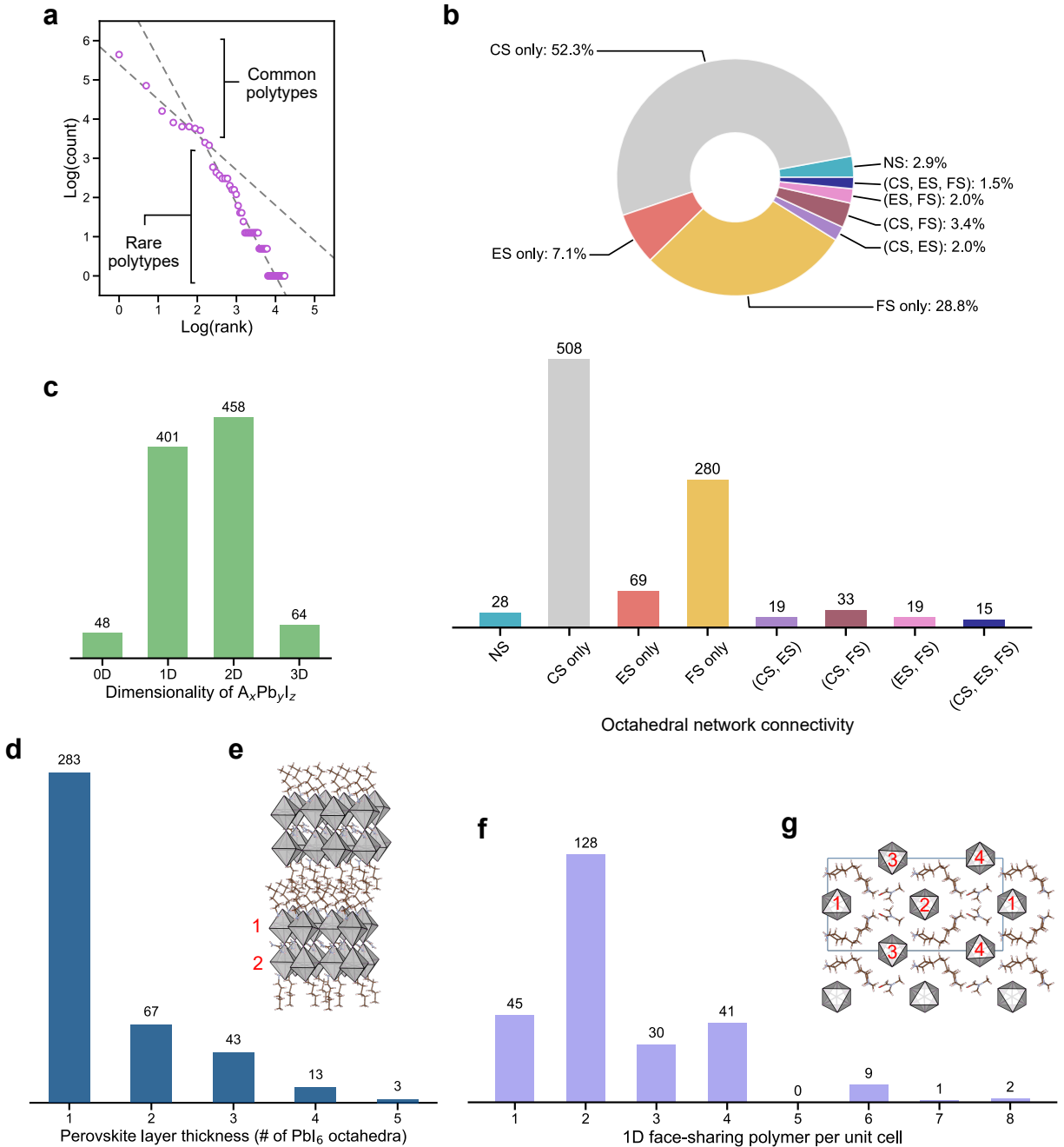


Figure 6: **Statistical summary of octahedral networks in $A_xPb_yI_z$.** **a**, The ranking distribution of the inorganic polytypes in the $A_xPb_yI_z$ dataset contains distinct regimes for common and rare polytypes in a log-log plot. **b**, Distribution of the structures differentiated by their PbI_6 octahedral connectivity types. Here, CS (corner-sharing) only, ES (edge-sharing) only, and FS (face-sharing) only include the structures with the respective unary connectivity type. NS indicates non-sharing. The structures containing mixed connectivity are divided into binary and ternary connectivity types and labeled with the constituent types in parentheses. **c**, Framework dimensionality of the structures. **d**, Distribution of the layer thickness in 2D layered perovskites (polytype name CS k -layer, $k = 1, 2, \dots$), along with an example structure in **e** showing a CS 2-layer polytype. **f**, Distribution of 1D FS chains per unit cell, along with an example structure in **g** showing four symmetry-independent FS chains per unit cell, which is indicated by the solid blue box.

octahedra, while some also contain CS octahedra co-existing with FS or ES octahedra in the same structure (Fig. 6b). The nearest-neighbor connectivity pattern of COs has the trend,

$$\text{corner-sharing PbI}_6 > \text{face-sharing PbI}_6 \gg \text{edge-sharing PbI}_6. \quad (1)$$

In terms of probability of connectivity (P), we can equivalently write $P_{\text{PbI}_6}^{\text{CS}} > P_{\text{PbI}_6}^{\text{FS}} \gg P_{\text{PbI}_6}^{\text{ES}}$. This observation violates Pauling’s third rule¹ for the structure prediction of ionic compounds, which orders corner-sharing (CS) as the most likely connectivity type between neighboring coordination environments, followed by edge-sharing (ES), and then face-sharing (FS). The violation leads to a modified preference in connectivity, which is observed in layered oxides,⁷¹ oxides under non-ambient conditions,⁷² and oxides with large anion size and high coordination number.³⁶ However, for halides, no systematic study is yet present.

For structural prediction, Pauling’s third rule still provides a good estimate for the *dominant* connectivity type between coordination environments,^{36,73} which is CS in our case for a homogeneously connected coordination network (i.e., containing only a single connectivity type). For those with two distinct connectivity types, our summary in Fig. 6b) shows that the polytype with coexisting CS and FS PbI₆ octahedra, the two main connectivity types in Eq. (1), is the most common, followed by the other two possibilities,

$$\text{corner- \& face-sharing PbI}_6 \gg \text{corner- \& edge-sharing PbI}_6 \sim \text{face- \& edge-sharing PbI}_6. \quad (2)$$

This may also be written more compactly in the probability of connectivity as $P_{\text{PbI}_6}^{\text{CS,FS}} \gg P_{\text{PbI}_6}^{\text{CS,ES}} \approx P_{\text{PbI}_6}^{\text{FS,ES}}$, and $P_{\text{PbI}_6}^{\text{CS,FS}} \propto P_{\text{PbI}_6}^{\text{CS}} P_{\text{PbI}_6}^{\text{FS}}$, similarly for the other two probabilities for mixed connectivity. Eq. (2) may be regarded as the second-order extension of Pauling’s third rule¹ for the specific type of coordination environment encountered here.

Structure occurrence and design principles. The polytype occurrence ranking in Fig. 5b reveals more information supplementary to the connectivity trends discussed in Eqs. (1)-(2). By cross-examination, we find a scarcity of structures with 2D layers entirely composed of edge-sharing PbI₆ octahedra (only 3 out of ~ 970). In contrast, the 2D edge-sharing motif is the majority polytype of PbI₂,⁷⁴ a parent compound of $A_x\text{Pb}_y\text{I}_z$, as well as the structure of the “analogous perovskite” compound BiI₃ (in the sense that ReO₃ is structurally analogous to ABO₃)⁷⁵ that has been reported.⁷⁶ This is likely due to the balance of charges since infinite edge-sharing PbI₆ octahedral layers are charge neutral and would require vacancies to bear charges¹³ and incorporate *A*-site cations. In fact, the more common types of ONs in $A_x\text{Pb}_y\text{I}_z$ with edge-sharing connectivity are predominantly 1D, featuring a short secondary unit, such as an edge-sharing 2-mer or 3-mer, stacked up through corner-sharing or edge-sharing (e.g., Fig. 5c₆). Impressively, the 1D multi-meric polytypes with a single connectivity type (i.e., only containing CS, ES, or FS octahedra),

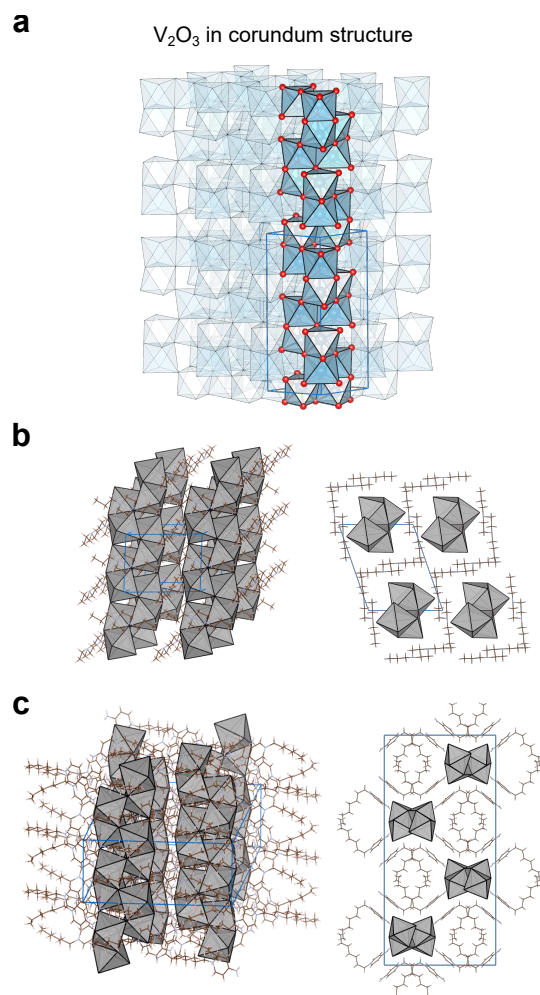


Figure 7: **Corundum-like columns in mixed-connectivity $A_xPb_yI_z$.** **a**, Illustration of the mixed connectivity columns (including corner-, edge-, and face-sharing simultaneously) in the corundum structure using V_2O_3 as an example. The cyan octahedra has the composition VO_6 and the oxygen atoms are in red. Similar columns with mixed connectivity exist in hybrid iodoplumbates, as in the examples **b**, $(C_{10}H_{24}N_2O)_2Pb_4I_{10}$ ⁶⁷ and **c**, $(C_{12}H_{21}N_2)_2Pb_2I_6$,⁶⁸ both shown in their respective side (left) and top (right) views. The blue box indicates the unit cell in all views.

traditionally found in materials with distinct oxidation states,⁷⁷ are all present within this single family of materials via pairing with different organic cations, indicating the tremendous framework variability of hybrid materials. These observations suggest that polyatomic organic cations can stabilize more diverse ONs than those typically found in the (parent) inorganic materials, where only monatomic cations exist.

In addition to rationalizing the observed trends, examination across polytypes with similar building units helps identify design principles related to (i) dimensionality tuning by changing connectivity, and (ii) building unit augmentation. For principle (i), we find that the dimensionality may be tuned by the octahedral connectivity within the inorganic framework. This enables the use

of ES or FS multimers to construct, in principle, ONs of any dimension (0D-3D), greatly expanding the perovskite motif with single CS octahedra. Although dimensional tuning has been discussed in the context of purely inorganic materials,⁷⁸ for hybrid metalates such as iodoplumbates, the vast space of admissible organic cations⁷⁹ suggests the possibility of fine-tuning the material properties by changing the inorganic framework. For principle (ii), we find that accommodation of the ON to different organic cations may also proceed by augmenting the secondary unit, such as from 1-mers or 2-mers to 6-mers, which are all found in the $A_xPb_yI_z$ dataset. Besides (unidirectional) stacking, which defines polytypism,⁵³ circular arrangements stand out as another distinguishing spatial construction.⁸⁰ The two principles outlined here are further discussed and illustrated with examples in Figs. S8-S9.

Discussions

From a computational perspective, our approach marries chemical intuition with geometry processing and the landscape of machine learning methods using object-centric representations.⁸¹ The objects here refer to the atom-centered COs present in the source data, rather than the atoms reported from simulation or experiment. Because of this object focus, the outcome is highly interpretable. The present work motivates further developments in efficient feature extraction methods. For example, existing approaches often require a symmetry-checking step^{39,82} that becomes computationally expensive for large datasets of complex structures. This necessitates simpler procedures followed by data cleaning using chemical intuition, which produces noisier data (e.g., with missed or inaccurately identified coordination environments). As such, the scalability of our approach is heavily dependent upon the efficiency and accuracy of coordination environment detection techniques.

From a materials chemistry perspective, our oxide and iodoplumbate results deserve further contemplation with regard to their published energetics and related material properties. Dimensional confinement effects,⁸³ which stem from changes in octahedral connectivity, significantly modify the electronic bandgap and optoelectronic properties in hybrid iodoplumbates and related ternary halides.^{23,84-86} In halide compositions, for instance, purely ES connectivity increases the bandgap by ~ 0.5 eV over purely CS connectivity, and FS increases the bandgap by another ~ 0.5 eV.⁸⁴ This is comparable to the bandgap broadening observed from compositional tuning by switching from iodide to bromide anions (~ 0.5 eV) and bromide to chloride anions (~ 0.6 eV).⁸⁷ Both effects are related to the reduced overlap of the atomic orbitals due to the lower dimensionality or the smaller anions. Moreover, the electronic dimensionality affects the photoluminescence properties of iodoplumbates: ES and FS motifs can lead to charge localization, which can enhance the photoluminescence quantum yield up to 100%.²⁵ On the contrary, CS and mixed-connectivity

motifs can be beneficial for charge transport and modified emissions (e.g., broad emission⁵²). For multinary hybrid metalates, the dimensionality and connectivity of their octahedral networks can also be altered by their synthesis conditions.⁶⁵

Conclusion and outlook

Our results demonstrate the advantage of task-dependent representations for machine learning-assisted exploration of the materials design space³³ and the need to explicitly incorporate connectivity information in existing distance-based representations.^{69,88} The diversity of ON motifs cataloged in the present work motivates further investigations into the relationship between connectivity patterns and application-specific materials properties^{89,90} computed with density functional theory. The CNE representation may be merged with those for organic molecules to build interpretable predictors and generative models of hybrid functional material properties. The modified Pauling’s third rule in the materials examined here and by others^{36,71–73} motivates its reformulation using a fully probabilistic approach that reflects chemical specificity and serves growing data. We envision a computational study whereby the functionalities could be tuned for a fixed ON, with pairing moieties that are optimized in an approach that resembles the docking mechanism in protein chemistry. Insights from such a study would facilitate targeted screenings for specific network connectivity patterns,⁹⁰ and likely reduce the resource cost and attrition rate from random search-based screening methods.⁹¹ It will grant us a broader accessible space using computational structure-prediction methods to systematically investigate new phases as well as material properties associated with connectivity modifications.

In addition to the materials studies in this work, our approach can also be adapted to extract insights from other analogous, yet less investigated materials families featuring ONs. They include inorganic and hybrid metalates with nonmetal or metalloid ligands, high-entropy materials,⁹² coordination polymers, and molecular perovskites,¹⁵ which possess even more complex design spaces and highly tunable structure-property landscapes. Our approach reflects the ongoing shift in materials design from an atom-centric perspective to one focused on coordination environment, which can capture the hierarchical organization of complex materials that gives rise to long-range order. This modular perspective supports the rational design of multinary and molecular perovskites, where collective polyhedral distortions dictate emerging optoelectronic functionality.^{15,26}

Methods

Materials datasets and their curation

The oxide perovskite (ABO_3) polymorph dataset was obtained from high-throughput computational screening of compositionally valid compounds. We provide here a summary of the computational method with further details reported elsewhere:⁴⁴ The structures of the oxide perovskites were generated using the software SPuDS,⁹³ which accounts for electrostatic structural distortions using bond-valence theory. The SPuDS-generated structures were further optimized using density functional theory within the Vienna Ab-initio Simulation Program (VASP 5.4.1) and under periodic boundary conditions utilizing projector augmented wave (PAW) pseudopotentials and the Perdew-Burke-Ernzerhof (PBE) generalized gradient approximation (GGA) exchange-correlation functional.⁹⁴ Electronic self-consistent field energies were converged to within 10^{-6} eV and forces were converged to within 0.01 eV/Å. The dataset is represented in the `pymatgen`-style json format.⁹⁵

The structural data for hybrid iodoplumbates ($A_xPb_yI_z$) were obtained from the Cambridge Structural Database (CSD),⁹⁶ accumulated until early 2022. We directly queried the CSD via a chemical search of lead and iodine compounds, which yielded over 1020 entries. We next removed entries that were not hybrid iodoplumbates, including (i) structures that did not contain organic components (removed by checking the chemical species beyond Pb and I in the compound) and (ii) structures with lead coordination environments other than octahedral (removed during the initial coordination environment detection). We also kept only the compounds with a Pb stoichiometry of up to 6 in the chemical formula. The final number of stoichiometrically-ordered data entries was 971, which includes fewer than 6 entries with duplicated IDs in the CSD. These duplicates were kept because of their different measurement conditions.

The majority of data processing was carried out using `crystmorph`, which implements the workflow described in SI section 1 for the analysis of ONs. We adopted a chemical environment parser⁸² to analyze the structures by iteratively identifying the space groups of possible coordination environments centered locally on every atom. For the structures used in this work, the analysis was performed only for metal-centered coordination environments to speed up the process. The coordination environment is partitioned into COs, which are the base objects in `crystmorph`. The algebraic operations between COs, as described in SI section 1, are implemented at either the atomic level (mesh graph) or the CO-level (inter-unit graph).

Naming rules for inorganic polytypes

There exist a few naming systems for modular (or recombination) materials, largely based on the fragments.^{48,53} For 3D frameworks, the notations from Ramsdell⁹⁷ and Jagodzinski⁹⁸ for polytypes have been used, yet they are limited to layer-stacking structures with a single chemical composition. These notations cannot concretely capture non-stacking structures (e.g., 0D structures)⁶¹ comprised of atom-centered COs with shared chemical origins as the parent compound. Moreover, hybrid materials contain distinct chemical components (e.g., inorganic and organic) and exhibit increased structural diversity from sublattice composition and mixing.^{99,100} Their description goes beyond the naming systems designed for purely inorganic (binary) compounds.^{2,101,102} The polytypism is only interpreted at the level of the inorganic sublattice,²⁶ hence inorganic polytypes. For hybrid iodoplumbates (and similarly for other halometalates), we can treat the $[Pb_yI_z]^{n-}$ part as a polyatomic ion derived from a polytypic binary compound, which forms the inorganic framework. The naming procedure is divided into the following rules.

1. **Degree of connectivity.** The *degree of connectivity* is defined as the number of shared vertices between two octahedra, which could be 0, 1, 2, or 3, for non-sharing (NS), corner-sharing (CS), edge-sharing (ES),

or face-sharing (FS), respectively. The naming starts from the octahedral units with the highest degree of connectivity and proceeds in decreasing order.

2. **Building units.** In atomic ONs, the *primary (building) units* of the structure are the COs with atomic ligands, the *secondary (building) units* are constructed from primary units through *gluing* operations¹⁰³ such as atom-sharing (i.e., corner, edge, face-sharing), which form *multimers*. Similarly, a *tertiary (building) unit* can be constructed from gluing secondary units through corner-, edge-, or face-sharing, or a mixture of them.

3. **Multiplicity of building units.** This step starts from identifying the smallest and most connected secondary unit (a multimer) within the ON. In graph-theoretical terms, this amounts to the maximally connected subgraph of the inter-unit graph representing the ON. Then, determine the *multiplicity* of the building units. For a multimeric structure, the multiplicity is the number of COs involved in the secondary unit. A *multimer* (or *k*-mer) has a secondary unit with a multiplicity of *k* (*k* is a positive integer). Naturally, a dimer, trimer, tetramer, and pentamer may be referred to as 2-mer, 3-mer, 4-mer, and 5-mer, respectively. Two limiting cases of the multiplicity exist: The lower limit ($k = 1$) is a *monomer*, such as the isolated 1-mers (OD structures)⁶¹ in Fig. 5. The upper limit ($k = \infty$) is a *polymer* or *polymeric chain* of octahedra, which is equivalent to an ∞ -mer (infinite-mer).

4. **Elementary and complex multimers.** A multimer can be corner-, edge-, or face-sharing, or have a mixture of them. They are called CS multimer, ES multimer, FS multimer, or mixed-connectivity multimer, respectively. An *elementary multimer* has only one type of connectivity, while a *complex multimer* has at least two types of connectivity.

5. **Decorated multimers.** A multimer can be *linear* (1D) or, equivalently, *flat* (2D), *zigzag* (1D) or, equivalently, *corrugated* (2D), *curved*, or *circular*, which are decorative terms to illustrate the fine features at larger spatial scales, typically requiring at least a 3-mer unit to represent. A straight multimer is the default type, so the adjective is dropped in its name, but for other types, the adjective is necessary. They are the corrugated *k*-mer, curved *k*-mer, or circular *k*-mer, respectively. In a corrugated multimer, the octahedral units are connected consecutively on alternating sides of the previous one.⁵² In a curved multimer, the octahedral units are getting progressively closer to the initial one, but are not forming a closed circular pattern.¹⁰⁴ In a circular multimer, the terminal octahedral unit forms a closure with the initial one through atom-sharing.^{80,105}

6. **Framework dimensionality.** An octahedral framework can be polymeric (1D *chain* or *polymer*), layered (2D *layer*), or scaffolded (3D *framework*). This level of specification naturally yields the dimensionality of the framework.^{48,106}

7. **Naming sequence.** The name of the inorganic framework is constructed sequentially from the primary unit (U_1) to the secondary unit (U_2) and above. The name is written as “ U_m of U_{m-1} of ... of U_2 of U_1 ”, with increasing hierarchy from U_1 to U_m .

The set of naming rules we propose here is meant for generating searchable polytype names and calculating summary statistics for a structure collection. They are based on the ON motifs and are constructed intuitively to account for the multiscale nature of the connectivity pattern present in the material structures. The polytype names produced from these rules contain explicit information of the inorganic framework, so are also usable as labels for machine learning tasks, such as predicting the connectivity types, the framework dimensionality, the multiplicity of building units, conditioned on the pairing moieties. The use of these naming rules is illustrated from the ground up with two real examples in Fig. S7. More examples of the named polytypes are given in Table S5.

We note here that these naming rules will not be able to cover all possible CO combinations or ON architectures, as their variability can grow exponentially, nor can any of the conventions that have been proposed so far in the crystallography community.^{10,48,53,98} However, our naming rules can handle the vast majority of cases for halometalates (and likely for related metalates) involving ONs and contain a level of generality within their designed scope.

Data availability statement

The single oxide perovskite polymorph dataset (structures) is available on GitHub ([link](#)). The hybrid iodoplumbate dataset (features, results, and IDs of Cambridge Structural Database) is provided in the supporting information.

Supporting information

- Extended details of the two structure analysis case studies (oxides and iodoplumbates), theoretical calculations of oxidation states, description of the computational workflow, and named examples for the inorganic polytypes illustrating their trends (PDF).
- Table S5: A selection of inorganic polytypes of $A_xPb_yI_z$ ranked by occurrence (PDF).
- Table S6: Results from unsupervised classification along with human-refined labels (XLSX).

Note

The authors declare no competing financial interest. The code for the analysis of octahedral networks is accessible on GitHub (<https://github.com/RealPolitiX/crystmorph>).

Acknowledgements

We thank G. Csányi (University of Cambridge) and H.-C. zur Loye (University of South Carolina) for helpful discussions. The work was supported by the Air Force Research Laboratory through the research grant (FA8655-21-1-7010). C.B.M. and R.J.M. were supported by the U.S. Department of Energy (DOE), Office of Energy Efficiency and Renewable Energy (EERE), Hydrogen and Fuel Cell Technologies Office (HFTO), and specifically the HydroGEN Advanced Water Splitting Materials Consortium, established as part of the Energy Materials Network under this same office (award DE-EE0008088). C.B.M. and R.J.M. also acknowledge support from the National Science Foundation (awards NSF CHEM-1800592 and CBET-2016225). I.H. acknowledges support from the Israel Science Foundation (Grant No. 2078/23). C.S. acknowledges start-up support from the University of South Carolina.

References

- (1) Pauling, L. The principles determining the structure of complex ionic crystals. *Journal of the American Chemical Society* **1929**, *51*, 1010–1026.
- (2) Wells, A. F. *Three-dimensional nets and polyhedra*; Wiley, 1977.
- (3) Férey, G. Building Units Design and Scale Chemistry. *Journal of Solid State Chemistry* **2000**, *152*, 37–48.
- (4) Ferraris, G.; Makovicky, E.; Merlino, S. *Crystallography of Modular Materials*; Oxford University Press, 2008.
- (5) Hawthorne, F. C. The structure hierarchy hypothesis. *Mineralogical Magazine* **2014**, *78*, 957–1027.
- (6) Bindi, L.; Nespolo, M.; Krivovichev, S. V.; Chapuis, G.; Biagioni, C. Producing highly complicated materials. Nature does it better. *Reports on Progress in Physics* **2020**, *83*, 106501.
- (7) Waroquiers, D.; Gonze, X.; Rignanese, G.-M.; Welker-Nieuwoudt, C.; Rosowski, F.; Göbel, M.; Schenk, S.; Degelmann, P.; André, R.; Glaum, R.; Hautier, G. Statistical Analysis of Coordination Environments in Oxides. *Chemistry of Materials* **2017**, *29*, 8346–8360.
- (8) Aleksandrov, K. S.; Beznosikov, V. V. Hierarchies of perovskite-like crystals (Review). *Physics of the Solid State* **1997**, *39*, 695–715.
- (9) Gregory, D. H. Nitride chemistry of the s-block elements. *Coordination Chemistry Reviews* **2001**, *215*, 301–345.
- (10) Müller, U. *Inorganic Structural Chemistry.*, 2nd ed.; Wiley, 2007.
- (11) Simon, A. Clusters of Valence Electron Poor Metals—Structure, Bonding, and Properties. *Angewandte Chemie International Edition in English* **1988**, *27*, 159–183.
- (12) Williams, G. R.; O’Hare, D. Towards understanding, control and application of layered double hydroxide chemistry. *Journal of Materials Chemistry* **2006**, *16*, 3065.
- (13) Saparov, B.; Mitzi, D. B. Organic–Inorganic Perovskites: Structural Versatility for Functional Materials Design. *Chemical Reviews* **2016**, *116*, 4558–4596.
- (14) Mao, L.; Teicher, S. M. L.; Stoumpos, C. C.; Kennard, R. M.; DeCrescent, R. A.; Wu, G.; Schuller, J. A.; Chabynyc, M. L.; Cheetham, A. K.; Seshadri, R. Chemical and Structural Diversity of Hybrid Layered Double Perovskite Halides. *Journal of the American Chemical Society* **2019**, *141*, 19099–19109.

- (15) Boström, H. L. B. Tilts and shifts in molecular perovskites. *CrystEngComm* **2020**, *22*, 961–968.
- (16) Cammarata, A.; Rondinelli, J. M. Covalent dependence of octahedral rotations in orthorhombic perovskite oxides. *The Journal of Chemical Physics* **2014**, *141*, 114704.
- (17) Voskanyan, A. A.; Navrotsky, A. Shear Pleasure: The Structure, Formation, and Thermodynamics of Crystallographic Shear Phases. *Annual Review of Materials Research* **2021**, *51*, 521–540.
- (18) Wells, A. F. The octahedron in chemistry. *Journal of Solid State Chemistry* **1973**, *6*, 469–478.
- (19) Hallweger, S. A.; Kaußler, C.; Kieslich, G. The structural complexity of perovskites. *Physical Chemistry Chemical Physics* **2022**, *24*, 9196–9202.
- (20) Filip, M. R.; Giustino, F. The geometric blueprint of perovskites. *Proceedings of the National Academy of Sciences* **2018**, *115*, 5397–5402.
- (21) Bartel, C. J.; Sutton, C.; Goldsmith, B. R.; Ouyang, R.; Musgrave, C. B.; Ghiringhelli, L. M.; Scheffler, M. New tolerance factor to predict the stability of perovskite oxides and halides. *Science Advances* **2019**, *5*, eaav0693.
- (22) Bare, Z. J. L.; Morelock, R. J.; Musgrave, C. B. Dataset of theoretical multinary perovskite oxides. *Scientific Data* **2023**, *10*, 244.
- (23) Stoumpos, C. C.; Mao, L.; Malliakas, C. D.; Kanatzidis, M. G. Structure–Band Gap Relationships in Hexagonal Polytypes and Low-Dimensional Structures of Hybrid Tin Iodide Perovskites. *Inorganic Chemistry* **2017**, *56*, 56–73.
- (24) Smith, M. D.; Crace, E. J.; Jaffe, A.; Karunadasa, H. I. The Diversity of Layered Halide Perovskites. *Annual Review of Materials Research* **2018**, *48*, 111–136.
- (25) Jin, J.-C.; Shen, N.-N.; Wang, Z.-P.; Peng, Y.-C.; Huang, X.-Y. Photoluminescent ionic metal halides based on s^2 typed ions and aprotic ionic liquid cations. *Coordination Chemistry Reviews* **2021**, *448*, 214185.
- (26) Gilley, I. W.; Wiggins, T. E.; Sargent, E. H.; Kanatzidis, M. G. Perovskitoids as Functional Materials. *Accounts of Chemical Research* **2025**, *58*, 2243–2254.
- (27) Taylor, Z. N. et al. Stabilization of O–O Bonds by d^0 Cations in $\text{Li}_{4+x}\text{Ni}_{1-x}\text{WO}_6$ ($0 \leq x \leq 0.25$) Rock Salt Oxides as the Origin of Large Voltage Hysteresis. *Journal of the American Chemical Society* **2019**, *141*, 7333–7346.

- (28) Wu, Y.; Shaker, S.; Brivio, F.; Murugavel, R.; Bristowe, P. D.; Cheetham, A. K. [Am]Mn(H₂POO)₃ : A New Family of Hybrid Perovskites Based on the Hypophosphite Ligand. *Journal of the American Chemical Society* **2017**, *139*, 16999–17002.
- (29) Glazer, A. M. The classification of tilted octahedra in perovskites. *Acta Crystallographica Section B Structural Crystallography and Crystal Chemistry* **1972**, *28*, 3384–3392.
- (30) Mercier, N. Hybrid Halide Perovskites: Discussions on Terminology and Materials. *Angewandte Chemie International Edition* **2019**, *58*, 17912–17917.
- (31) Akkerman, Q. A.; Manna, L. What Defines a Halide Perovskite? *ACS Energy Letters* **2020**, *5*, 604–610.
- (32) He, Q.; Ishikawa, R.; Lupini, A. R.; Qiao, L.; Moon, E. J.; Ovchinnikov, O.; May, S. J.; Biegalski, M. D.; Borisevich, A. Y. Towards 3D Mapping of BO₆ Octahedron Rotations at Perovskite Heterointerfaces, Unit Cell by Unit Cell. *ACS Nano* **2015**, *9*, 8412–8419.
- (33) Onat, B.; Ortner, C.; Kermode, J. R. Sensitivity and dimensionality of atomic environment representations used for machine learning interatomic potentials. *The Journal of Chemical Physics* **2020**, *153*, 144106.
- (34) Musil, F.; Grisafi, A.; Bartók, A. P.; Ortner, C.; Csányi, G.; Ceriotti, M. Physics-Inspired Structural Representations for Molecules and Materials. *Chemical Reviews* **2021**, *121*, 9759–9815.
- (35) Botsch, M.; Kobbelt, L.; Pauly, M.; Alliez, P.; Levy, B. *Polygon Mesh Processing*; A K Peters/CRC Press, 2010.
- (36) George, J.; Waroquiers, D.; Di Stefano, D.; Petretto, G.; Rignanese, G.; Hautier, G. The Limited Predictive Power of the Pauling Rules. *Angewandte Chemie International Edition* **2020**, *59*, 7569–7575.
- (37) Bechtel, J. S.; Van der Ven, A. Octahedral tilting instabilities in inorganic halide perovskites. *Physical Review Materials* **2018**, *2*, 025401.
- (38) Filip, M. R.; Eperon, G. E.; Snaith, H. J.; Giustino, F. Steric engineering of metal-halide perovskites with tunable optical band gaps. *Nature Communications* **2014**, *5*, 5757.
- (39) Ganose, A. M.; Jain, A. Robocrystallographer: automated crystal structure text descriptions and analysis. *MRS Communications* **2019**, *9*, 874–881.

- (40) Saidi, W. A.; Shadid, W.; Castelli, I. E. Machine-learning structural and electronic properties of metal halide perovskites using a hierarchical convolutional neural network. *npj Computational Materials* **2020**, *6*, 36.
- (41) Straus, D. B.; Guo, S.; Abeykoon, A. M.; Cava, R. J. Understanding the Instability of the Halide Perovskite CsPbI₃ through Temperature-Dependent Structural Analysis. *Advanced Materials* **2020**, *32*, 2001069.
- (42) Sun, W.; Dacek, S. T.; Ong, S. P.; Hautier, G.; Jain, A.; Richards, W. D.; Gamst, A. C.; Persson, K. A.; Ceder, G. The thermodynamic scale of inorganic crystalline metastability. *Science Advances* **2016**, *2*.
- (43) Goldschmidt, V. M. Die Gesetze der Krystallochemie. *Die Naturwissenschaften* **1926**, *14*, 477–485.
- (44) Morelock, R. J.; Bare, Z. J. L.; Musgrave, C. B. Bond-Valence Parameterization for the Accurate Description of DFT Energetics. *Journal of Chemical Theory and Computation* **2022**, *18*, 3257–3267.
- (45) Goodenough, J. B. Electronic and ionic transport properties and other physical aspects of perovskites. *Reports on Progress in Physics* **2004**, *67*, 1915–1993.
- (46) Gschneidner, K. A. *Handbook on the Physics and Chemistry of Rare Earths Vol. 50*; 2016; pp 1–18.
- (47) Mitzi, D. B. Templating and structural engineering in organic–inorganic perovskites. *Journal of the Chemical Society, Dalton Transactions* **2001**, 1–12.
- (48) Lima-de Faria, J.; Hellner, E.; Liebau, F.; Makovicky, E.; Parthé, E. Nomenclature of inorganic structure types. Report of the International Union of Crystallography Commission on Crystallographic Nomenclature Subcommittee on the Nomenclature of Inorganic Structure Types. *Acta Crystallographica Section A Foundations of Crystallography* **1990**, *46*, 1–11.
- (49) Krivovichev, S. V.; Filatov, S. K.; Semenova, T. F. On the systematics and description of polyions of linked polyhedra. *Zeitschrift für Kristallographie - Crystalline Materials* **1997**, *212*, 411–417.
- (50) Cao, D. H.; Stoumpos, C. C.; Farha, O. K.; Hupp, J. T.; Kanatzidis, M. G. 2D Homologous Perovskites as Light-Absorbing Materials for Solar Cell Applications. *Journal of the American Chemical Society* **2015**, *137*, 7843–7850.
- (51) Soe, C. M. M. et al. Structural and thermodynamic limits of layer thickness in 2D halide perovskites. *Proceedings of the National Academy of Sciences* **2019**, *116*, 58–66.

- (52) Mao, L.; Wu, Y.; Stoumpos, C. C.; Wasielewski, M. R.; Kanatzidis, M. G. White-Light Emission and Structural Distortion in New Corrugated Two-Dimensional Lead Bromide Perovskites. *Journal of the American Chemical Society* **2017**, *139*, 5210–5215.
- (53) Guinier, A.; Bokij, G. B.; Boll-Dornberger, K.; Cowley, J. M.; Āurovič, S.; Jagodzinski, H.; Krishna, P.; de Wolff, P. M.; Zvyagin, B. B.; Cox, D. E.; Goodman, P.; Hahn, T.; Kuchitsu, K.; Abrahams, S. C. Nomenclature of polytype structures. Report of the International Union of Crystallography Ad hoc Committee on the Nomenclature of Disordered, Modulated and Polytype Structures. *Acta Crystallographica Section A Foundations of Crystallography* **1984**, *40*, 399–404.
- (54) Mercier, N.; Louvain, N.; Bi, W. Structural diversity and retro-crystal engineering analysis of iodometalate hybrids. *CrystEngComm* **2009**, *11*, 720.
- (55) Wu, L.-M.; Wu, X.-T.; Chen, L. Structural overview and structure–property relationships of iodoplumbate and iodobismuthate. *Coordination Chemistry Reviews* **2009**, *253*, 2787–2804.
- (56) Qian, J.; Guo, Q.; Liu, L.; Xu, B.; Tian, W. A theoretical study of hybrid lead iodide perovskite homologous semiconductors with 0D, 1D, 2D and 3D structures. *Journal of Materials Chemistry A* **2017**, *5*, 16786–16795.
- (57) Deng, Z.; Kieslich, G.; Bristowe, P. D.; Cheetham, A. K.; Sun, S. Octahedral connectivity and its role in determining the phase stabilities and electronic structures of low-dimensional, perovskite-related iodoplumbates. *APL Materials* **2018**, *6*, 114202.
- (58) Blatov, V. A. Voronoi–dirichlet polyhedra in crystal chemistry: theory and applications. *Crystallography Reviews* **2004**, *10*, 249–318.
- (59) Klain, D. A.; Rota, G.-C. *Introduction to geometric probability*; Cambridge University Press, 1997.
- (60) Naskręcki, B.; Jaskolski, M.; Dauter, Z. The Euler characteristic as a basis for teaching topology concepts to crystallographers. *Journal of Applied Crystallography* **2022**, *55*, 154–167.
- (61) Sun, S.; Lu, M.; Gao, X.; Shi, Z.; Bai, X.; Yu, W. W.; Zhang, Y. 0D Perovskites: Unique Properties, Synthesis, and Their Applications. *Advanced Science* **2021**, *8*, 2102689.
- (62) Bibal, A.; Frénay, B. Measuring Quality and Interpretability of Dimensionality Reduction Visualizations. *Safe Machine Learning workshop at International Conference on Learning Representations* **2019**,

- (63) Hennig, C. What are the true clusters? *Pattern Recognition Letters* **2015**, *64*, 53–62.
- (64) Mitzenmacher, M. A Brief History of Generative Models for Power Law and Lognormal Distributions. *Internet Mathematics* **2003**, *1*, 226–251.
- (65) Daub, M.; Hillebrecht, H. From 1D to 3D: Perovskites within the System $\text{HSC}(\text{NH}_2)_2\text{I} / \text{CH}_3\text{NH}_3\text{I} / \text{PbI}_2$ with Maintenance of the Cubic Closest Packing. *Inorganic Chemistry* **2021**, *60*, 3082–3093.
- (66) Nellikkal, M. A. N.; Keeseey, R.; Zeile, M.; Shekar, V.; Li, Z.; Leiby, N.; Zeller, M.; Chan, E. M.; Schrier, J.; Norquist, A. J. Spatiotemporal Route to Understanding Metal Halide Perovskitoid Crystallization. *Chemistry of Materials* **2022**, *34*, 5386–5396.
- (67) Hou, Q.; Bai, F.-Q.; Jia, M.-J.; Jin, J.; Yu, J.-H.; Xu, J.-Q. New organically templated chained and layered iodoplumbates. *CrystEngComm* **2012**, *14*, 4000–4007.
- (68) Duan, H.-B.; Yu, S.-S.; Tong, Y.-B.; Zhou, H.; Ren, X.-M. Two in one: switchable ion conductivity and white light emission integrated in an iodoplumbate-based twin chain hybrid crystal. *Dalton Transactions* **2016**, *45*, 4810–4818.
- (69) Bartók, A. P.; Kondor, R.; Csányi, G. On representing chemical environments. *Physical Review B* **2013**, *87*, 184115.
- (70) Cheng, B.; Griffiths, R.-R.; Wengert, S.; Kunkel, C.; Stenczel, T.; Zhu, B.; Deringer, V. L.; Bernstein, N.; Margraf, J. T.; Reuter, K.; Csanyi, G. Mapping Materials and Molecules. *Accounts of Chemical Research* **2020**, *53*, 1981–1991.
- (71) Delmas, C.; Fouassier, C.; Hagenmuller, P. Structural classification and properties of the layered oxides. *Physica B+C* **1980**, *99*, 81–85.
- (72) Bykova, E.; Bykov, M.; Černok, A.; Tidholm, J.; Simak, S. I.; Hellman, O.; Belov, M. P.; Abrikosov, I. A.; Liermann, H.-P.; Hanfland, M.; Prakapenka, V. B.; Prescher, C.; Dubrovinskaya, N.; Dubrovinsky, L. Metastable silica high pressure polymorphs as structural proxies of deep Earth silicate melts. *Nature Communications* **2018**, *9*, 4789.
- (73) Pathak, R.; Sharma, M. K.; Biswas, K. Pauling's Third Rule as a Guide for Designing Low Thermal Conducting Chalcogenides. *Chemistry of Materials* **2025**, *37*, 4227–4235.
- (74) Beckmann, P. A. A review of polytypism in lead iodide. *Crystal Research and Technology* **2010**, *45*, 455–460.
- (75) Evans, H. A.; Wu, Y.; Seshadri, R.; Cheetham, A. K. Perovskite-related ReO_3 -type structures. *Nature Reviews Materials* **2020**, *5*, 196–213.

- (76) Brandt, R. E.; Kurchin, R. C.; Hoye, R. L. Z.; Poindexter, J. R.; Wilson, M. W. B.; Sulekar, S.; Lenahan, F.; Yen, P. X. T.; Stevanović, V.; Nino, J. C.; Bawendi, M. G.; Buonassisi, T. Investigation of Bismuth Triiodide (BiI_3) for Photovoltaic Applications. *The Journal of Physical Chemistry Letters* **2015**, *6*, 4297–4302.
- (77) Rouxel, J., Ed. *Crystal Chemistry and Properties of Materials with Quasi-One-Dimensional Structures*; Springer Netherlands: Dordrecht, 1986.
- (78) Tulsy, E. G.; Long, J. R. Dimensional Reduction: A Practical Formalism for Manipulating Solid Structures. *Chemistry of Materials* **2001**, *13*, 1149–1166.
- (79) Karimitari, N.; Baldwin, W. J.; Muller, E. W.; Bare, Z. J. L.; Kennedy, W. J.; Csányi, G.; Sutton, C. Accurate Crystal Structure Prediction of New 2D Hybrid Organic–Inorganic Perovskites. *Journal of the American Chemical Society* **2024**, *146*, 27392–27404.
- (80) Krautscheid, H.; Vielsack, F. Discrete and polymeric iodoplumbates with Pb_3I_{10} building blocks: $[\text{Pb}_3\text{I}_{10}]^{4-}$, $[\text{Pb}_7\text{I}_{22}]^{8-}$, $[\text{Pb}_{10}\text{I}_{28}]^{8-}$, ${}^1_{\infty}[\text{Pb}_3\text{I}_{10}]^{4-}$ and ${}^2_{\infty}[\text{Pb}_7\text{I}_{18}]^{4-}$. *Journal of the Chemical Society, Dalton Transactions* **1999**, 2731–2735.
- (81) Grohe, M. word2vec, node2vec, graph2vec, X2vec: Towards a Theory of Vector Embeddings of Structured Data. Proceedings of the 39th ACM SIGMOD-SIGACT-SIGAI Symposium on Principles of Database Systems. New York, NY, USA, 2020; pp 1–16.
- (82) Waroquiers, D.; George, J.; Horton, M.; Schenk, S.; Persson, K. A.; Rignanese, G.-M.; Gonze, X.; Hautier, G. ChemEnv : a fast and robust coordination environment identification tool. *Acta Crystallographica Section B Structural Science, Crystal Engineering and Materials* **2020**, *76*, 683–695.
- (83) Hoye, R. L. Z.; Hidalgo, J.; Jagt, R. A.; Correa-Baena, J.; Fix, T.; MacManus-Driscoll, J. L. The Role of Dimensionality on the Optoelectronic Properties of Oxide and Halide Perovskites, and their Halide Derivatives. *Advanced Energy Materials* **2022**, *12*, 2100499.
- (84) Kamminga, M. E.; de Wijs, G. A.; Havenith, R. W. A.; Blake, G. R.; Palstra, T. T. The Role of Connectivity on Electronic Properties of Lead Iodide Perovskite-Derived Compounds. *Inorganic Chemistry* **2017**, *56*, 8408–8414.
- (85) Mauck, C. M.; Tisdale, W. A. Excitons in 2D Organic–Inorganic Halide Perovskites. *Trends in Chemistry* **2019**, *1*, 380–393.
- (86) Liu, A.; Zhu, H.; Bai, S.; Reo, Y.; Caironi, M.; Petrozza, A.; Dou, L.; Noh, Y.-Y. High-performance metal halide perovskite transistors. *Nature Electronics* **2023**, *6*, 559–571.

- (87) Marchenko, E. I.; Fateev, S. A.; Petrov, A. A.; Korolev, V. V.; Mitrofanov, A.; Petrov, A. V.; Goodilin, E. A.; Tarasov, A. B. Database of Two-Dimensional Hybrid Perovskite Materials: Open-Access Collection of Crystal Structures, Band Gaps, and Atomic Partial Charges Predicted by Machine Learning. *Chemistry of Materials* **2020**, *32*, 7383–7388.
- (88) Banjade, H. R.; Hauri, S.; Zhang, S.; Ricci, F.; Gong, W.; Hautier, G.; Vucetic, S.; Yan, Q. Structure motif-centric learning framework for inorganic crystalline systems. *Science Advances* **2021**, *7*, eabf1754.
- (89) Dyer, M. S.; Collins, C.; Hodgeman, D.; Chater, P. A.; Demont, A.; Romani, S.; Sayers, R.; Thomas, M. F.; Claridge, J. B.; Darling, G. R.; Rosseinsky, M. J. Computationally Assisted Identification of Functional Inorganic Materials. *Science* **2013**, *340*, 847–852.
- (90) Park, Y.; Kim, S. H.; Lee, D.; Lee, J.-S. Designing zero-dimensional dimer-type all-inorganic perovskites for ultra-fast switching memory. *Nature Communications* **2021**, *12*, 3527.
- (91) Oganov, A. R.; Pickard, C. J.; Zhu, Q.; Needs, R. J. Structure prediction drives materials discovery. *Nature Reviews Materials* **2019**, *4*, 331–348.
- (92) Musicó, B. L.; Gilbert, D.; Ward, T. Z.; Page, K.; George, E.; Yan, J.; Mandrus, D.; Kepens, V. The emergent field of high entropy oxides: Design, prospects, challenges, and opportunities for tailoring material properties. *APL Materials* **2020**, *8*, 040912.
- (93) Lufaso, M. W.; Woodward, P. M. Prediction of the crystal structures of perovskites using the software program SPuDS. *Acta Crystallographica Section B Structural Science* **2001**, *57*, 725–738.
- (94) Perdew, J. P.; Burke, K.; Ernzerhof, M. Generalized Gradient Approximation Made Simple. *Physical Review Letters* **1996**, *77*, 3865–3868.
- (95) Ong, S. P.; Richards, W. D.; Jain, A.; Hautier, G.; Kocher, M.; Cholia, S.; Gunter, D.; Chevrier, V. L.; Persson, K. A.; Ceder, G. Python Materials Genomics (pymatgen): A robust, open-source python library for materials analysis. *Computational Materials Science* **2013**, *68*, 314–319.
- (96) Groom, C. R.; Bruno, I. J.; Lightfoot, M. P.; Ward, S. C. The Cambridge Structural Database. *Acta Crystallographica Section B Structural Science, Crystal Engineering and Materials* **2016**, *72*, 171–179.
- (97) Li, Z.; Park, J.-S.; Walsh, A. Evolutionary exploration of polytypism in lead halide perovskites. *Chemical Science* **2021**, *12*, 12165–12173.

- (98) Kunz, S. L.; Haefner, M.; Clemens, O. “Hexagonal” Perovskites: From Stacking Sequence to Space Group Symmetry and New Opportunities. *Chemistry of Materials* **2024**, *36*, 11341–11358, Publisher: American Chemical Society.
- (99) Bartel, C. J.; Clary, J. M.; Sutton, C.; Vigil-Fowler, D.; Goldsmith, B. R.; Holder, A. M.; Musgrave, C. B. Inorganic Halide Double Perovskites with Optoelectronic Properties Modulated by Sublattice Mixing. *Journal of the American Chemical Society* **2020**, *142*, 5135–5145.
- (100) Wiggins, T. E.; Bati, A. S. R.; Kepenekian, M.; Reynolds, R. P.; Zeiske, S.; Pournara, A. D.; Liu, C.; Yang, Y.; Zhang, X.; Gilley, I. W.; Chen, B.; Even, J.; Sargent, E. H.; Kanatzidis, M. G. Pb:Sn Ratio-Driven Polytypism and Band Modulation in Photoresponsive Hexagonal Perovskitoids. *Journal of the American Chemical Society* **2025**, *147*, 21014–21031.
- (101) Müller, U. MX₄-Ketten aus kantenverknüpften Oktaedern: mögliche Kettenkonfigurationen und mögliche Kristallstrukturen. *Acta Crystallographica Section B Structural Crystallography and Crystal Chemistry* **1981**, *37*, 532–545.
- (102) Burdett, J. K.; McLarnan, T. J. Geometrical and electronic links among the structures of MX₂ solids: structural enumeration and electronic stability of pyritelike systems. *Inorganic Chemistry* **1982**, *21*, 1119–1128.
- (103) Gallier, J. Notes on Convex Sets, Polytopes, Polyhedra, Combinatorial Topology, Voronoi Diagrams and Delaunay Triangulations. arXiv May 2, 2008; <https://doi.org/10.48550/arXiv.0805.0292>, accessed 2026-03-03.
- (104) Mishra, S.; Jeanneau, E.; Daniele, S.; Ledoux, G.; Swamy, P. N. Solid- and Solution Phase Transformations in Novel Hybrid Iodoplumbate Derivatives Templated by Solvated Yttrium Complexes. *Inorganic Chemistry* **2008**, *47*, 9333–9343.
- (105) Yue, C.-Y.; Sun, H.-X.; Liu, Q.-X.; Wang, X.-M.; Yuan, Z.-S.; Wang, J.; Wu, J.-H.; Hu, B.; Lei, X.-W. Organic cation directed hybrid lead halides of zero-dimensional to two-dimensional structures with tunable photoluminescence properties. *Inorganic Chemistry Frontiers* **2019**, *6*, 2709–2717.
- (106) Hoffmann, R. Small but Strong Lessons from Chemistry for Nanoscience. *Angewandte Chemie International Edition* **2013**, *52*, 93–103.